Faraday Discuss., 1996, **104**, 209–229

Phase transitions in monolayers of medium-chain alcohols on water studied by sum-frequency spectroscopy and ellipsometry

Brian D. Casson, Rüdiger Braun and Colin D. Bain*

Physical and Theoretical Chemistry Laboratory, South Parks Rd., Oxford, UK OX1 3QZ

Monolayers of medium-chain alcohols $CH_3(CH_2)_{m-1}OH$ ($m = 9$–14) have been studied by sum-frequency vibrational spectroscopy and ellipsometry in the vicinity of the two-dimensional solid–liquid phase transition. *Gauche* defects are present in the solid phase and increase only slightly in the monolayer just above the phase transition. A model of the chains as freely rotating rigid rods permits a calculation of the area per molecule and chain tilt in the liquid phase. The density of the hydrocarbon chains in the liquid monolayer phase is less than that in the solid monolayer phase but significantly higher than in a bulk liquid alkane. The area per molecule, chain tilt and volume per CH_2 group in the liquid phase all increase with increasing chain length.

1 Introduction

It is more than a century since Pockels[1] first reported the manipulation of insoluble monolayers spread on water and 80 years since Langmuir's pioneering studies on phase transitions in these films.[2] Since then Adam, Harkins, Dervichian, Stenhagen, Lundquist, Pethica and Peterson, amongst many others, have identified a rich phase diagram in Langmuir–Pockels monolayers.[3] The nature of many of these phases remained a mystery until the advent of grazing incidence X-ray diffraction from monolayers on water.[4,5] It is now possible to determine the unit cell parameters and even the molecular orientation within the monolayer. On the basis of this knowledge, an extensive correspondence between monolayer phases and the bulk phases of smectic liquid crystals and crystalline alkanes has been identified.[6]

Much less attention has been devoted to phase transitions in monolayers of soluble surfactants. Indeed, there is a view that first-order phase transitions do not occur in soluble monolayers.[7] Solubility, however, is an unsatisfactory parameter for categorising surfactants, since the definition of insoluble is arbitrary and depends greatly on the timescale, τ, of the measurement. For example, a monolayer that is soluble on a Langmuir trough (τ *ca.* mins) may be insoluble in a light scattering experiment (τ *ca.* μs). To avoid this problem, we use the term 'adsorbed' rather than 'soluble' to refer to a monolayer that is in thermodynamic equilibrium with the bulk solution. Insoluble monolayers are prepared by spreading a solution of the amphiphile in an organic solvent onto the water surface and are, in general, metastable with respect to the three-dimensional crystal: only below the equilibrium spreading pressure (ESP) of the hydrated crystal can a Langmuir–Pockels monolayer be at thermodynamic equilibrium. Conversely, adsorbed monolayers can only sample those parts of the phase diagram that lie below the ESP. Although the ESP of some long-chain amphiphiles (in particular, fatty acids) is very low, a range of equilibrium solid phases† do exist, for example, in alcohols, esters

† We use the term 'solid' loosely to refer to both crystalline monolayers and mesophases showing quasi-long range orientational correlations and 'liquid' to refer to monolayers in which all correlations exhibit rapid exponential decay.

and shorter fatty acids.[3e,3f,8] One might then ask why so few phase transitions have been identified with 'soluble' surfactants. One argument against the widespread existence of solid–liquid phase transitions in adsorbed monolayers is that many surfactants form micelles in solution and that micelles require chain flexibility for their stability. Micelle formation therefore limits the surface pressure to a value that is too low for crystalline monolayers to form. The absence of a liquid–vapour phase transition requires that the monolayer is above its two-dimensional critical temperature. The rather low value of the critical temperature in insoluble monolayers of fatty acids[3e] certainly lent credibility to this view. Recent measurements on pentadecanoic acid demonstrated that the critical temperature is much higher than previously thought,[9] suggesting that amphiphiles with shorter chains may also show liquid–gas phase transitions. Indeed, Aratono *et al.* have reported a first-order liquid–vapour phase transition in a range of adsorbed monolayers, including octanol, octanoic acid and sodium dodecyl sulfate,[10] though their claims have been disputed.[7]

The presence of a first-order phase transition in adsorbed monolayers of medium-chain alcohols on water at high surface pressures has been demonstrated unequivocally.[11–16] This phase transition has also been identified in monolayers of alcohols at the oil/water[17] and solid/water interface.[18] Crystalline monolayers have been detected at the surface of liquid alkanes within a few degrees of their freezing points,[19] and in monolayers of sodium dodecyl sulfate on water.[20] These studies show that the existence of a bulk phase in equilibrium with a monolayer does not preclude crystalline monolayer phases, and indeed these can exist in equilibrium with the bulk liquid. A surface phase transition has even been reported in a fully miscible binary mixture of acetonitrile and water.[21] It thus appears that phase transitions in adsorbed monolayers may be more widespread than has previously been appreciated.

In this paper, we present a study of the first-order phase transition in adsorbed monolayers of medium-chain alcohols, $CH_3(CH_2)_{m-1}OH$ ($m = 9$–14), on water. This phase transition was first reported in 1993 by Berge and Renault who observed a discontinuity in the ellipsometric phase angle, Δ, and in the first derivative of the surface tension at temperatures well above the melting point of the bulk alcohols.[11] Grazing incidence X-ray diffraction measurements showed that below the phase-transition temperature, $T_m(2D)$, the monolayers had a hexagonal unit cell of area 21.5 Å^2 with the chains oriented nearly normal to the surface.[12,13] These data suggest that the 'solid' phase has a structure analogous to the rotator II phase found in bulk alkanes. Above $T_m(2D)$ (the 'liquid' phase) no Bragg scattering was observed. Berge and co-workers also inferred the area per molecule in the liquid phase from a thermodynamic analysis of surface tension measurements.[14] Recently, Rieu *et al.* estimated the density and roughness of the monolayers in both phases by X-ray reflectivity.[15]

Despite these experiments, much remains to be learnt about the liquid phase of the monolayers. Vibrational spectroscopy is one way of probing the structure on a molecular scale in both phases. The method we use is sum-frequency spectroscopy (SFS), which is particularly sensitive to conformational order in hydrocarbon chains. SFS is a nonlinear optical technique in which the surface of water is irradiated simultaneously with a visible and an IR laser and the light emitted at the sum of two input frequencies is detected (Fig. 1).[22–24] Scanning the IR frequency generates a vibrational spectrum of molecules at the air/water interface. Only modes that are both IR and Raman-active are observed. Fig. 2 shows an example of SF spectra from a monolayer of dodecanol for all three independent polarisation combinations: ssp, ppp and sps, where the labels refer to the polarisation of the sum-frequency, visible and IR fields, in that order. Fig. 3 shows SF spectra of undecanol above and below the phase-transition temperature. The intensity of the strongest peak in Fig. 3 (the symmetric methyl stretch) changes discontinuously at the phase transition. The intensity of this peak depends on the area per molecule, A, and chain tilt, χ, in the monolayer. To separate these two effects we

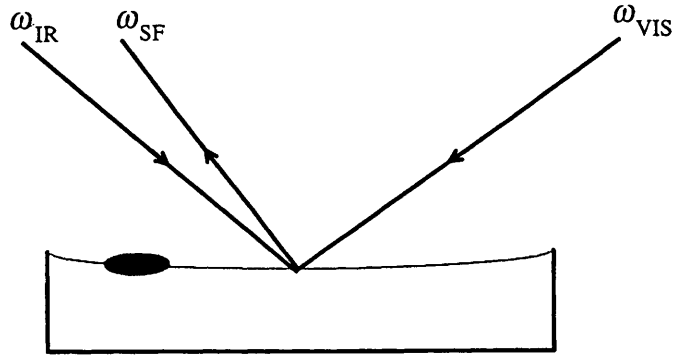

Fig. 1 Schematic illustration of the experimental geometry for SFS. The monolayer is in equilibrium with a lens of liquid alcohol on the water surface.

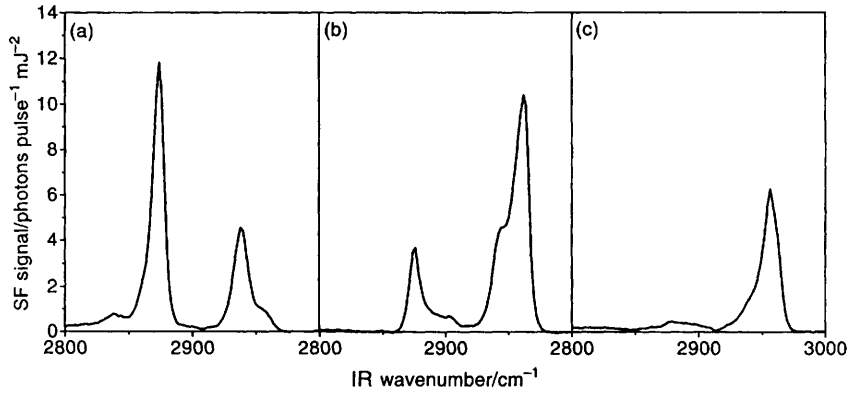

Fig. 2 SF spectra in the C—H stretching region of a monolayer of dodecanol on water at 20 °C. (a) ssp polarisation (b) ppp polarisation (c) sps polarisation.

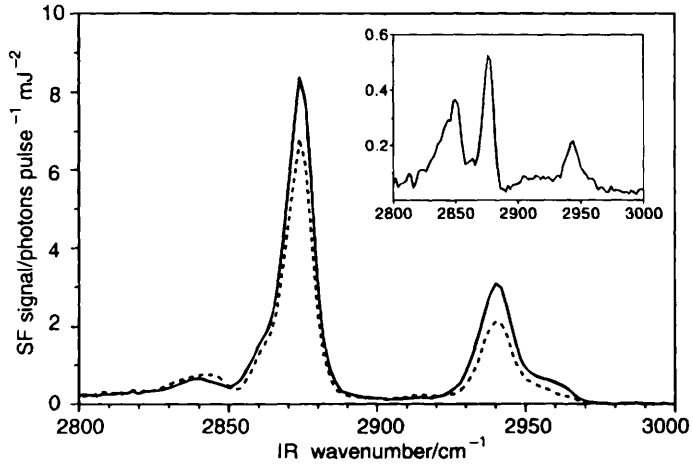

Fig. 3 SF spectra with ssp polarisation of a monolayer of undecanol on water just below (——) and just above (— —) the phase transition at 28 °C. Inset: SF spectrum of a monolayer of the soluble surfactant $CH_3(CH_2)_{11}(OC_2H_4)_3OH$ at an area per molecule of 37 Å^{2}.[66]

combine SFS with a complementary experimental technique, ellipsometry. In ellipsometry, we determine the change in polarisation of a light beam reflected from the surface. The property we measure, the coefficient of ellipticity, $\bar{\rho}$, depends most sensitively on the density of the monolayer: $\bar{\rho}$ increases as A increases, but decreases as the tilt increases. In contrast, the SF intensity decreases when either A or χ increases. The two techniques therefore respond differently to changes in the structure of the monolayer.

In a previous communication,[16] we reported SF and ellipsometry data for one chain length, undecanol. In this paper, we develop a more sophisticated analysis of the ellipsometric data and extend our study to all the alcohols with chain lengths between 9 and 14 carbons.

2 Theoretical background to ellipsometry

Ellipsometry is a well established technique that has frequently been used to analyse organic monolayers on water,[25] yet it has only recently become possible to interpret ellipsometric data from monolayers quantitatively.[26] There are two reasons for this advance. First, the existence of reliable molecular areas from X-ray diffraction experiments reduces the number of unknown variables. Second, developments in the theory of ellipsometry now permit a correct treatment of roughness[27] and anisotropy in the monolayer.[28] The theory that we require for the analysis of the experimental data in this paper is summarised here.

The coefficient of ellipticity, $\bar{\rho}$, of a surface is defined as $\mathrm{Im}(r_p/r_s)$ at the Brewster angle, θ_B, where r_p and r_s are the reflection coefficients for p and s-polarised light, respectively.[29] θ_B is the angle where $\mathrm{Re}(r_p/r_s) = 0$. In the limit where the thickness, d, of a monolayer is very much less than the wavelength, λ, of light, $\bar{\rho}$ is determined by a single ellipsometric parameter, η, characterising the interface.[30]

$$\bar{\rho} = \frac{\pi}{\lambda} \frac{\sqrt{(\varepsilon_1 + \varepsilon_2)}}{\varepsilon_1 - \varepsilon_2} \eta \tag{1}$$

where ε_1 and ε_2 are the relative permittivities of air and water, respectively, at the wavelength of the light source. η can be broken down into a term due to the thickness of the monolayer, η^d and a term due to the roughness of the interface, η^R. These two terms can be treated independently.[31]

A detailed discussion of the effect of roughness in ellipsometry at the Brewster angle has been given recently by Meunier.[31] η^R arises from multiple scattering of the incident light by thermally excited capillary waves. Croce[32] has shown that

$$\eta^R = -\frac{3}{2} \frac{(\varepsilon_1 - \varepsilon_2)^2}{\varepsilon_1 + \varepsilon_2} \sum_{2\pi/\lambda}^{q_{max}} q \langle \zeta_q^2 \rangle \tag{2}$$

where ζ_q is the amplitude of the capillary wave with wavevector $\boldsymbol{q}$. Similar expressions have been obtained by Beaglehole[33] and Zielinska *et al.*[34] ζ_q is given by equipartition as

$$\langle \zeta_q^2 \rangle = \frac{kT}{\rho g + \gamma q^2 + K q^4} \tag{3}$$

where ρ is the density of the liquid, g the acceleration due to gravity, γ the surface tension and K the bending modulus. For the wavevectors $q > 2\pi/\lambda$ that affect the ellipticity, the gravitational term is negligible and η^R is determined by γ, K and the upper limit on the summation in eqn. (2). If $K \gg kT$, capillary waves with high q (*i.e.* short wavelength and therefore high curvature) are suppressed, the upper limit of the summation can be extended to infinity and the summation evaluated to give

$$\eta^R = -\frac{3}{2} \frac{(\varepsilon_1 - \varepsilon_2)^2}{\varepsilon_1 + \varepsilon_2} \frac{kT}{2\pi\gamma} q_e \tag{4}$$

where $q_e = (\pi/2)\sqrt{(\gamma/K)}$. If $K = 0$ and the capillary waves are treated as independent then the summation in eqn. (2) diverges, unless an empirical cut-off is introduced. This limit is usually taken to be a molecular length scale, q_{mol}^{-1}, beyond which the continuum description of capillary waves breaks down. We then have eqn. (4) with $q_e = q_{mol}$. Meunier[27] has shown that if one allows for mode coupling between capillary waves at high q, γ and K become functions of q and the summation over q converges without the necessity for the introduction of an arbitrary cut-off. For $K \ll kT$, $q_e = (\pi/2)\sqrt{(8\pi\gamma/3kT)}$ and hence

$$\eta^R = -\frac{3}{2}\frac{(\varepsilon_1 - \varepsilon_2)^2}{\varepsilon_1 + \varepsilon_2}\sqrt{\left(\frac{\pi kT}{6\gamma}\right)} \tag{5}$$

For crystalline films, an upper limit to the summation in eqn. (2) is provided by the lattice parameter, a, even in the coupled-wave model: $q_{max} = \pi/a$. Integration over q then yields

$$q_e = \sqrt{\left(\frac{8\pi\gamma}{3kT}\right)}\tan^{-1}\left[\frac{\pi}{a}\sqrt{\left(\frac{3kT}{8\pi\gamma}\right)}\right] \tag{6}$$

Eqn. (6) predicts $\bar{\rho}^R \approx +0.4 \times 10^{-3}$ for monolayers of n-alcohols on water, for which $a = 5$ Å and $\gamma \approx 30$ mN m^{-1} at the phase transition.[11,12] In addition to capillary wave roughness, there may be a positive contribution to $\bar{\rho}^R$ from the intrinsic roughness of the monolayer caused by intrachain defects and tilt disorder.[35]

To evaluate the thickness term, η^d, we treat the molecules in the monolayer as rigid rods that are uniformly tilted by an angle, χ from the surface normal. The thickness, d, of the monolayer is taken to be $md_0 \cos\chi$, where m is the number of methylene units in the chain and $d_0 = 1.27$ Å is the length per CH_2 group of a fully extended hydrocarbon chain. We assume that the hydroxy head group has the same relative permittivity as water and ignore the terminal hydrogen of the methyl group.

In a free rotator phase the chains are uniaxial with polarisability volumes, α'_e and α'_0, parallel and perpendicular to the optical (chain) axis. The components of the relative permittivity tensor, ε_e and ε_0, are evaluated from eqn. (7):[36]

$$\varepsilon_{e,0} - 1 = \frac{4\pi n\alpha'_{e,0}}{1 - 4\pi n\alpha'_{e,0}L_{e,0}} \tag{7}$$

where n = number of molecules per unit volume = $(Amd_0 \cos\chi)^{-1}$, and L_0 and L_e are the diagonal elements of the Lorentz tensor. In an isotropic or cubic material the Lorentz factors are equal and have the value 1/3.

The azimuthal direction of the tilt, χ, will vary from domain to domain. If the tilt direction is random and the size of the domains is small compared with the diameter of the HeNe laser beam, then the monolayer will behave as a uniaxial film with its optical axis perpendicular to the surface of the water. Under these conditions[31]

$$\eta^d = \frac{\varepsilon_e\varepsilon_0 + (\varepsilon_0 \sin^2\chi + \varepsilon_e \cos^2\chi)[\varepsilon_0 - 2(\varepsilon_1 + \varepsilon_2)] + 2\varepsilon_1\varepsilon_2}{2(\varepsilon_0 \sin^2\chi + \varepsilon_e \cos^2\chi)} md_0 \cos\chi \tag{8}$$

Below the phase-transition temperature, the tilt angle, χ determined by X-ray diffraction is close to zero.[13] Then[37]

$$\eta^d = \frac{(\varepsilon_e - \varepsilon_1)(\varepsilon_e - \varepsilon_2)}{\varepsilon_e} md_0 + (\varepsilon_0 - \varepsilon_e)md_0 \tag{9}$$

The first term is the ellipsometric parameter[30] for an isotropic monolayer with relative permittivity, ε_e, and is positive if $\varepsilon_e > \varepsilon_1, \varepsilon_2$. The second term is a correction for the anisotropy, and is negative for positive uniaxial monolayers.

3 Experimental

Details of the SF spectrometer[24] and experimental procedure[38,39] may be found elsewhere. The visible beam (532 nm, 4 ns, 10 mJ pulse^{-1}, 2 mm diameter, 20 Hz, angle of incidence $\theta_i = 55°$) and the IR beam (3000–2800 cm^{-1}, *ca.* 1 ns, 0.7–1 mJ pulse^{-1}, 0.4 mm diameter, $\theta_i = 50°$) were overlapped on the surface of the sample in a counter-propagating geometry. The SF signal was detected with a liquid N_2-cooled CCD camera (Princeton Instruments CCD-512-TKB) and normalised to a reference SF signal obtained simultaneously from a GaAs crystal.

Samples were prepared by placing a drop or crystal of the alcohol on the surface of pure D_2O in a 50 mm diameter glass Petri dish. For nonanol, a 15 wt.% solution of NaCl in D_2O was used to depress the freezing point. The alcohol rapidly spreads to cover the whole surface. A control experiment in which a drop of dodecanol was placed on a saturated dodecanol solution yielded identical results: 2D mass transport rapidly replaces molecules lost from the monolayer by evaporation or diffusion into the bulk solution. The sample dishes were placed in a rotating holder mounted in a temperature-controlled stage with a heated lid containing a slit for entry and exit of the laser beams. For tridecanol and tetradecanol a CaF_2 window was employed to reduce further the evaporation of D_2O. Temperatures were measured by a Chromel–Alumel thermocouple with a precision of ± 0.1 °C and an absolute accuracy of ± 0.5 °C. Heating and cooling rates were typically 1–2 °C h^{-1}. Between three and eight heating and cooling cycles were measured for each alcohol.

The ellipsometric measurements were performed on a Beaglehole Instruments ellipsometer (Wellington, NZ) incorporating photoelastic modulation of an HeNe laser (633 nm) at 50 kHz and lock-in detection of the reflected light at 50 and 100 kHz. All experiments were performed at the Brewster angle. The same sample cell was used as in the SF experiments, but without sample rotation and with a subphase of ultra-high-purity H_2O (Elga). Between two and six heating and cooling cycles were measured for each alcohol. For nonanol, a 7.4 wt.% solution of NaCl in H_2O was employed.

The *n*-alcohols (>99% pure) were obtained from Larodan (Malmo, Sweden) and were used as received. D_2O was obtained from Aldrich. We checked the cleanliness of all glassware by measuring the ellipticity of ultrapure water placed in the glassware. Sodium chloride (BDH, 99.9%) was roasted in an oven at 500 °C to burn off any organic impurities.

In the SF experiments, the surface of water is pumped with a high-intensity IR laser beam. It is therefore essential to address the effect of sample heating on the SF spectra. The effect of both steady-state and transient heating on the SF spectra are discussed in the Appendix. We evaluated the effect of transient heating experimentally by defocusing the IR laser beam. In Fig. 4, we plot the intensity of the r^+ mode in a monolayer of decanol as a function of temperature for two different intensities of the IR beam differing by a factor of thirty. The phase-transition temperature, change in intensity at the phase transition and the relative slopes above and below T_m(2D) are all reproduced to within experimental error. This result gives us confidence that sample heating does not distort the experimental results.

4 Results

We will present first the data obtained from monolayers of decanol–tetradecanol, for which the phase-transition temperatures we observe are in excellent agreement with literature values. Our observations on monolayers of nonanol differ from those reported by Berge and co-workers[11–15] and so we address this molecule independently at the end of the section.

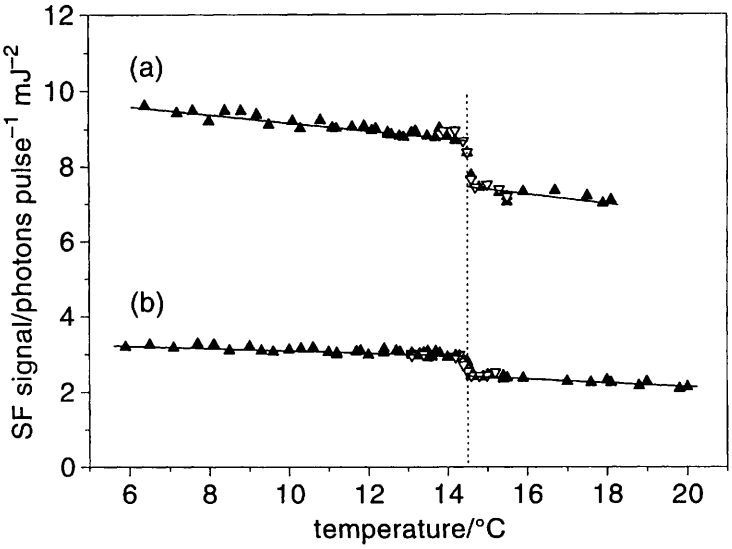

Fig. 4 SF signal at 2878 cm^{-1} for a monolayer of decanol on water as a function of temperature (ssp polarisation). Area of IR spot: (a) 0.1 and (b) 3 mm^2. (▲) Heating cycles and (▽) cooling cycles. The lines represent a linear fit to the data above and below T_m(2D).

4.1 SF spectroscopy

Fig. 2 shows SF spectra in the C—H stretching region of a monolayer of dodecanol in the solid phase for the three independent polarisation combinations. The major peaks can all be assigned to the terminal methyl group (see Table 1 for assignments and peak positions).[40] An all-*trans* hydrocarbon chain has local inversion symmetry; the methylene modes separate into an IR-active and Raman-active set and are therefore inactive in SFS. The weak methylene features near 2845 and 2880–2920 cm^{-1} arise from conformational defects still present in the solid phase. The commonest chain defects in dense monolayers are kinks (*gtg'* sequences) and end-*gauche* conformations.[41] Kinks are locally centrosymmetric, and therefore SF-inactive, and the CH_2 group α to the OH appears at higher frequencies. The methylene peaks therefore probably arise from *gauche* defects at the methyl terminus. The SF spectra of the other alcohols below their phase transition temperatures are similar to dodecanol.

Fig. 3 shows ssp-polarised SF spectra of undecanol on either side of the phase transition. The intensity of the d^+ methylene mode is almost unchanged while the intensity of the methyl modes decreases across the phase transition. The same change in intensity was measured for the strongest modes of undecanol in all three polarisations, to within

Table 1 Wavenumbers and mode assignments of peaks observed in SF spectra of monolayers of medium-chain alcohols on water[40]

mode	description	wavenumber/cm^{-1}
r^+	symmetric CH_3 stretch	2878
r^+FR	symmetric CH_3 stretch (Fermi resonance)	2942
r^-	antisymmetric CH_3 stretch	2956–2965
d^+	symmetric CH_2 stretch	2845
d^+FR	symmetric CH_2 stretch (Fermi resonance)	2880–2920

experimental error. A detailed analysis of conformational disorder requires isotopically labelled chains and is beyond the scope of this paper. We will restrict ourselves here to analysing the decrease in the SF signal from the methyl groups, ΔI_{SF}, at the phase transition. Since the change in intensity of the d^+ peak at the phase transition is small, we will neglect the effect of end-*gauche* defects on the intensity of the methyl modes[16] and interpret ΔI_{SF} in terms of just two variables: the area per molecule, A, and the tilt, χ, of the hydrocarbon chain.

In principle, both A and χ can be deduced from SF spectra acquired with different polarisations. In practice, we cannot determine both parameters, with the accuracy required, from SF experiments alone.[38] It is, however, possible to interpret the intensity of the r^+ mode in ssp-polarised spectra in terms of coupled changes in both A and χ with a degree of confidence. Fig. 5 shows the intensity of the r^+ mode in ssp-polarised spectra as a function of temperature for the five alcohols from decanol to tetradecanol. In each case, the intensity decreases linearly with temperature above and below $T_m(2D)$. The transition is <0.1 K wide (see inset in Fig. 5). Typically there was no hysteresis in the data, although occasionally supercooling of the molten monolayer was observed. The change in intensity at the phase transition, $\Delta I_{SF} = 1 - I_{SF}(\text{liquid})/I_{SF}(\text{solid})$ is reported in Table 2.

The intensity of the SF signal depends on three properties of the monolayer: the area per molecule, A; the molecular hyperpolarisability averaged over the orientations of the molecules in the monolayer, $\langle\beta\rangle$ and the Fresnel coefficients, $L_{SF}(\text{loc})$, $K_{VIS}(\text{loc})$ and $K_{IR}(\text{loc})$, which relate the incident and emitted fields to the local electric fields in the monolayer.[16]

$$I_{SF} \propto A^{-2}\langle\beta\rangle^2 L_{SF}^2(\text{loc}) K_{VIS}^2(\text{loc}) K_{IR}^2(\text{loc}) I_{VIS}\, I_{IR} \tag{10}$$

Assuming C_{3v} symmetry, there are only two independent Cartesian components of β for the r^+ mode: β_{ccc} and $\beta_{aac} = \beta_{bbc}$, where the axes $\boldsymbol{a}$ and $\boldsymbol{b}$ are perpendicular to the C_{3v} symmetry axis, $\boldsymbol{c}$. Only one component of the susceptibility, $\chi^{(2)}_{yyz}$, contributes to the

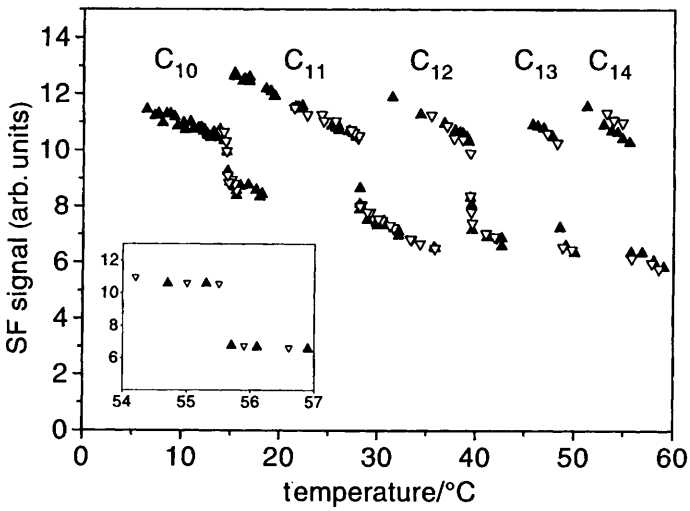

Fig. 5 SF signal at the peak of the r^+ stretch in ssp-polarised spectra of monolayers of five alcohols on water. (▲) Heating cycles and (▽) cooling cycles. The curves have been normalised to a value of 10 just below $T_m(2D)$. Inset: data for a monolayer of tetradecanol close to the phase-transition temperature, showing the sharpness of the phase transition and the lack of hysteresis.

Table 2 Phase-transition temperature, change in SF signal at the phase transition, and change in the coefficient of ellipticity at the phase transition for monolayers of alcohols with chain lengths between 10 and 14

m	T_m(2D)/K	$(\Delta I_{SF} \pm 1.4)$ (%)[a]	$(\Delta\bar{\rho} \pm 0.02)$ $(\times 10^{-3})$[a]
10	14.5	16.1	0.32
11	28.0	26.4	0.45
12	39.1	29.8	0.59
13	48.6	33.5	0.71
14	55.5	36.6	0.91

[a] Errors at 2σ level.

ssp-polarised spectra. After averaging over azimuthal angles in the plane of the water surface, we obtain for $\langle\beta_{yyz}\rangle$:[42]

$$\langle\beta_{yyz}\rangle = \frac{\beta_{aac}}{8}\left\{\langle\cos\theta\rangle\left(7+\frac{1}{r}\right)+\langle\cos 3\theta\rangle\left(1-\frac{1}{r}\right)\right\} \tag{11}$$

where $r = \beta_{aac}/\beta_{ccc}$ and θ is the angle between the C_3-axis and the surface normal.

For a rotator phase, $\langle\cos\theta\rangle = \langle\cos\chi\rangle\cos\alpha$, where α is the angle between the methyl group axis and the chain axis. An analogous expression may be derived for $\langle\cos 3\theta\rangle$.[16] Although there is some debate over the value of r,[43,16] this uncertainty has little effect on the analysis. Since $r \gg 1$ and the second term in eqn. (11) is typically only a few per cent of the first, $\langle\beta\rangle$ is given to a good approximation by $\frac{7}{8}\beta_{aac}\langle\cos\chi\rangle\cos\alpha$, independent of r. The full expression [eqn. (11)] was used in the analysis with $r = 3.4$.[16]

Expressions for the Fresnel coefficients in eqn. (10) have been given previously in terms of isotropic local field factors, which can in turn be expressed in terms of A and χ.[16] While an anisotropic treatment of the monolayer would be more accurate, the added complexity is not justified by the simplicity of the model. The contribution of local field effects to ΔI_{SF} is, in the event, rather small (<4%).

We have used eqn. (10) to compute a function $\chi_l(A_l)$ in the liquid phase that yields the correct value of ΔI_{SF}, assuming that $A_s = 21.5$ Å^2 and $\chi_s = 0°$ just below the phase-transition temperature and that the monolayer is homogeneous. Two representative curves are shown in Fig. 6.

4.2 Ellipsometry

In Fig. 7 we plot the coefficient of ellipticity, $\bar{\rho}$, for monolayers of decanol to tetradecanol. Each alcohol shows a sharp jump in $\bar{\rho}$ at the phase-transition temperature. The size of the step, $\Delta\bar{\rho}$, increases with increasing chain length (Table 2). The phase-transition temperatures are in excellent agreement with those obtained by SF spectroscopy and with literature values (Table 2).

The first step in the interpretation of the ellipticity is the determination of the roughness contribution, $\bar{\rho}^R$, and the optical constants of the solid monolayer, ε_e and ε_0. On the basis of published X-ray diffraction data,[13] the alcohols are believed to be isostructural just below their transition temperatures, with vertical chains and an area per molecule of 21.5 Å^2. Thus, if we plot $\bar{\rho}$ just below T_m(2D) as a function of chain length, m, we might expect a linear plot with intercept $\bar{\rho}^R$ and slope $\bar{\rho}^d$ per CH_2 group. The expressions for $\bar{\rho}$, however, contain the relative permittivity of water, ε_2, which varies with temperature.[44] To correct for this temperature dependence we need to know $\bar{\rho}^R$, ε_e and ε_0. Thus we adopt an iterative procedure in which we guess a value of $\bar{\rho}^R$ and then find values of ε_e

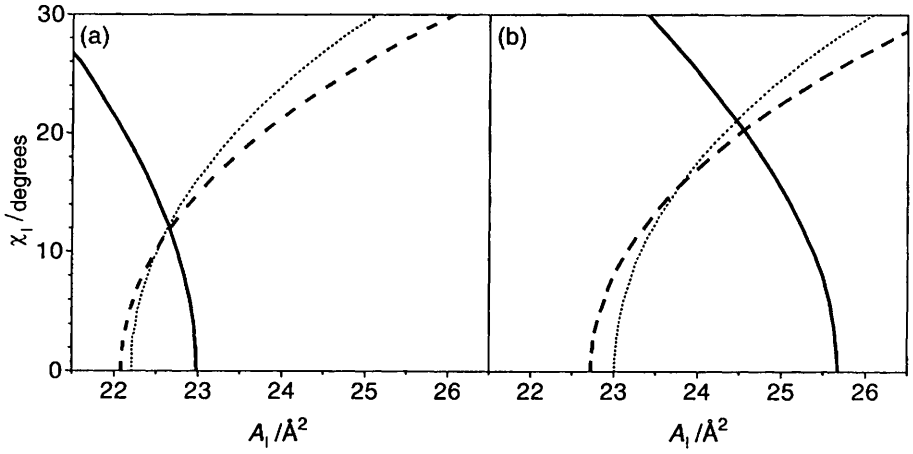

Fig. 6 Calculated curves of the chain tilt, χ_1, against the area per molecule, A_1, in the liquid phase, assuming that the solid phase just below the phase-transition temperature is homogeneous with an area per molecule of 21.5 Å^2 and a chain tilt of 0° (indicated by the origin in the plots), and that the molecules in the liquid phase can be treated as freely rotating rigid rods: (a) decanol (b) tetradecanol. SF data (——), ellipsometric data assuming an anisotropic monolayer (— —), ellipsometric data assuming an isotropic monolayer (· · ·).

and ε_0 that reproduce the observed slope of $\bar{\rho}^d = \bar{\rho} - \bar{\rho}^R$ against chain length, after correction of $\bar{\rho}^d$ to 298 K. The intercept is used to derive an improved estimate of $\bar{\rho}^R$ and the procedure is repeated. Clearly, it is not possible to determine two independent parameters, ε_e and ε_0, from a single experimental observation, the slope of $\bar{\rho}^d$ against m: additional information is required. In the 1940s, Vogel carried out a series of very careful measurements on liquid alkanes to determine the molar refractivity of CH_2 and CH_3 groups at several wavelengths. His data[45] yield a value for the mean polarisability

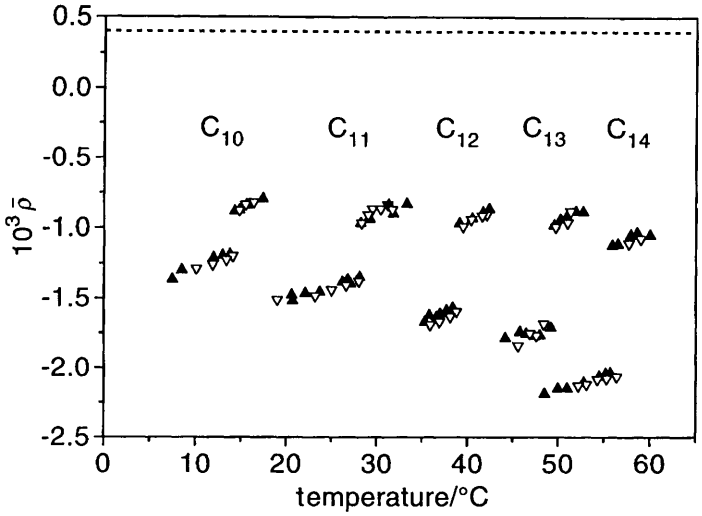

Fig. 7 Coefficient of ellipticity of monolayers of five alcohols on water as a function of temperature. The dotted line indicates the calculated value of $\bar{\rho}^R$. (▲) Heating cycles and (▽) cooling cycles.

volume $\overline{\alpha'} = \frac{1}{3}\,\mathrm{Tr}(\alpha') = 1.83$ Å^3 at 633 nm for a CH_2 unit. [This value of $\overline{\alpha'}$ was also used to evaluate the Fresnel coefficients in eqn. (12)]. In our analysis, we constrain $\overline{\alpha'}$ to Vogel's value and allow only the polarisability anisotropy, $\alpha'_e - \alpha'_0$, to vary. Since the Clausius–Mossotti relationship, from which molar refractivities are derived, assumes $L_e = L_0 = 1/3$ we use these Lorentz factors to calculate ε_e and ε_0 from $\overline{\alpha'}$ [eqn. (7)].

Fig. 8 shows the raw ellipticity and the ellipticity after correction for roughness and temperature. The iterations rapidly converge to yield a value of $\bar{\rho}^R = +0.4 \times 10^{-3}$. The slope of $\bar{\rho}^d = -0.16 \times 10^{-3}$ per CH_2 group yields optical constants $\varepsilon_e = 2.29$ and $\varepsilon_0 = 2.12$. The resulting values of ε_e and ε_0 are not, however, unique: had we chosen a different value of $\overline{\alpha'}$ we would have obtained equally good agreement with the experimental data but with a different anisotropy. Indeed, even an isotropic model with $\varepsilon = 2.01$ would fit, although a refractive index of 1.42 is unreasonably low for a hydrocarbon with a density of 0.85 g cm^{-3}.

To check the results of our analysis, we have compared the anisotropy of the alcohol monolayers ($\varepsilon_e = 2.29$; $\varepsilon_0 = 2.12$) with the observed birefringence of crystalline polyethylene ($\varepsilon_e = 2.50$; $\varepsilon_0 = 2.31$)[46] and of Langmuir monolayers of behenic acid in the solid phase ($\varepsilon_e = 2.37$; $\varepsilon_0 = 2.16$):[26] the agreement is excellent. As a further test of consistency, we measured the temperature dependence of $\bar{\rho}$ in tetradecanol monolayers between 40 and 55 °C. Using the linear expansion coefficient measured by Berge *et al.*[12] of 1×10^{-3} K^{-1}, we predict $\mathrm{d}\bar{\rho}/\mathrm{d}T = 2.9 \times 10^{-5}$ K^{-1}, compared to the experimental value of 2.8×10^{-5} K^{-1}.

With values of α'_e and α'_0 in hand, we can now use eqn. (1), (7) and (8) to calculate $\bar{\rho}^d$ as a function of area per molecule and chain tilt. We have employed isotropic Lorentz factors, but the results are the same if an ellipsoidal cavity with the dimensions of the C_2H_4 sub-cell is used to calculate L_e and L_0.[36] A second function $\chi_1(A_1)$ that reproduces the observed step, $\Delta\bar{\rho}$, at the phase transition was calculated for all five alcohols. The curves for decanol and tetradecanol are shown in Fig. 6. The intersection of the curves calculated from ellipsometry and SF spectroscopy yields the area per molecule and chain tilt in the liquid phase. The results are collected in Table 3. In Fig. 6 we have also

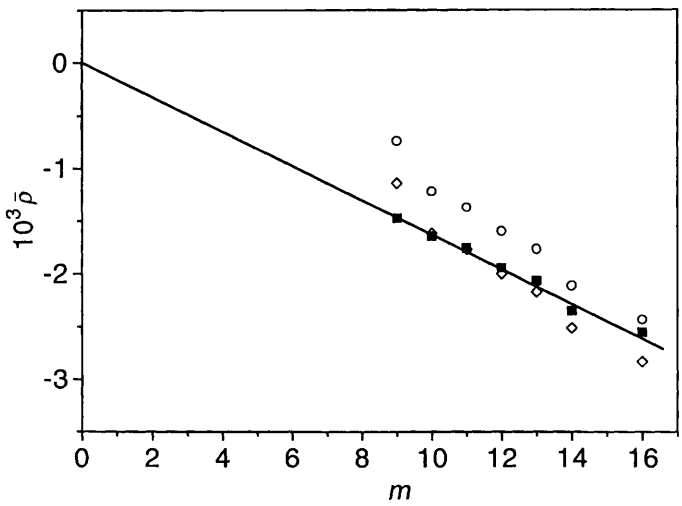

Fig. 8 Coefficient of ellipticity just below T_m(2D) as a function of chain length, m. For hexadecanol the phase transition is at 68 °C. Raw ellipticity (○), ellipticity after subtracting a roughness contribution $\bar{\rho}^R = 0.4 \times 10^{-3}$ (◇), ellipticity after correcting ε_2 to its value at 298 K and, in the case of nonanol, correcting for the effect of salt on ε_2 (■).

Table 3 Properties of the liquid phase of monolayers of alcohol with chain lengths between 10 and 14 carbons: area per molecule, change in area per molecule at the phase transition, and tilt (assuming $A_s = 21.5$ Å^2, $\chi_s = 0°$)

m	$(A_l \pm 10.15)$/Å^2 [a]	$(\Delta A \pm 0.7)$ (%)[a]	$\chi_l \pm 1$/degrees[a]
10	22.7	5.6	11.9[b]
11	23.5	9.3	17.0
12	23.8	10.7	18.0
13	24.2	12.6	19.5
14	24.5	14.0	20.3

[a] Errors at 2σ level. [b] Error = $\pm 1.5°$.

shown the curve we would obtain if we were to assume an isotropic monolayer with $\varepsilon = 2.01$. From this curve we deduce that A_l and χ_l are insensitive to a small error in the assumed value of $\overline{\alpha'}$.

4.3 Nonanol

Finally, we briefly address the phase transition in monolayers of nonanol. Berge reported a phase-transition temperature of $+2\,°C$ from ellipsometric and surface tension measurements.[11] We were unable to find evidence for a phase transition at temperatures above $-2\,°C$ either by ellipsometry or by SFS. Recently, we have made observations at lower temperatures on concentrated salt solutions and located a broad transition at -3 to $-5\,°C$. The origin of the discrepancy between our results and those of Berge *et al.* is unclear, though the salinities were not the same. Ellipsometric data for nonanol monolayers are shown in Fig. 10. The change in the coefficient of ellipticity, $\Delta\bar{\rho}$, at the phase

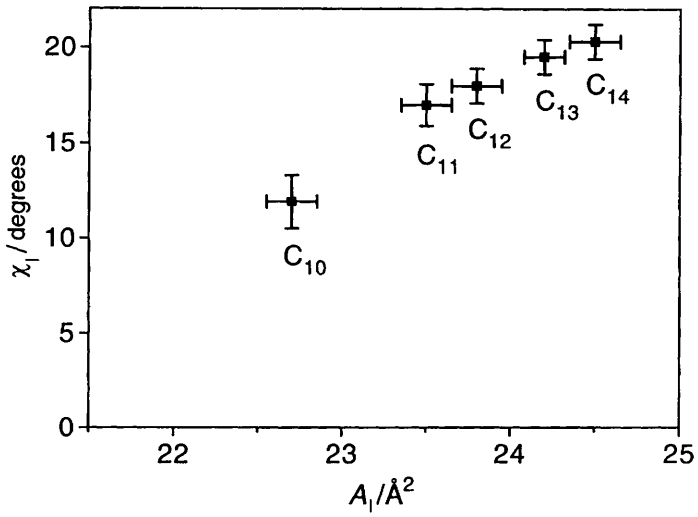

Fig. 9 Area per molecule and chain tilt in the liquid phase of monolayers of the five alcohols, $C_{10}OH$ to $C_{14}OH$, obtained from the intersection of the solid and dashed lines in Fig. 6 and equivalent plots for the other monolayers. The origin corresponds to the structure of the solid phase of the monolayer. Error bars are estimates at the 2σ level.

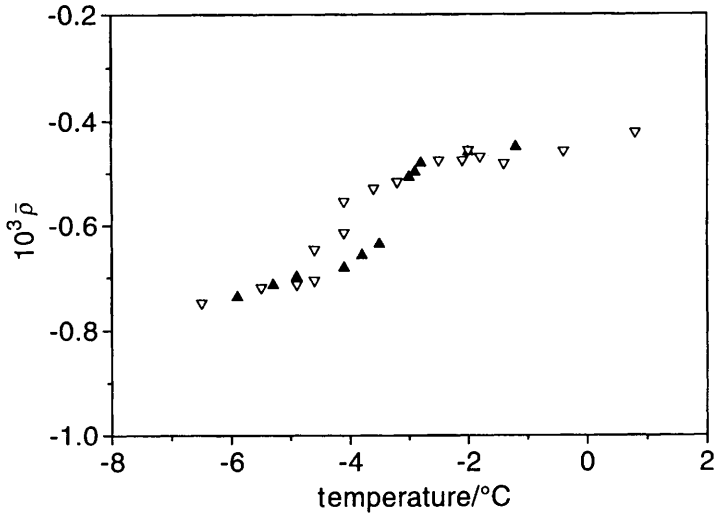

Fig. 10 Coefficient of ellipticity of a monolayer of nonanol on a 7.4 wt.% solution of NaCl in water. (▲) Heating cycle and (▽) cooling cycle.

transition is $<0.2 \times 10^{-3}$ and the corresponding change, ΔI_{SF}, in the SF spectrum is no more than 5%. From these preliminary data we estimate that $\Delta A \approx 2\%$ and $\chi_1 < 10°$. The behaviour of the ellipticity in the transition region is markedly different from that observed with higher alcohols, where the ellipticity at T_m(2D) oscillates between the values of the solid and liquid phases as domains drift through the laser beam. For nonanol, readings also fluctuate in the transition region but adopt values intermediate between those of the solid and liquid phases.

5 Discussion

5.1 Solid phase

Our analysis of the ellipticity of the monolayers below the phase transition generates a consistent model that not only give reasonable values for the optical constants but also gives the correct dependence on temperature and salinity. The experimental value of the roughness term, $\bar{\rho}^R$, is in excellent agreement with the coupled-mode capillary wave theory of Meunier for a non-rigid interface.[27] We would not expect a rotator phase to have a large bending modulus and indeed the value $K = 0.6\ kT$ one computes in the uncoupled description [eqn. (4)] is typical of microemulsion interfaces where the surfactant film is in a liquid phase.[47] Tilt disorder contributes little to roughness, since the chains are nearly vertical, and the concentration of defects, though not negligible, is probably much less than one per chain (Fig. 2).[16,41] Consequently, we would expect σ_0 to be small ($\ll 1$ Å), as observed.

SF spectroscopy is sensitive to conformational order in surfactant monolayers. The intensity of the CH_2 symmetric stretch confirms the presence of a small population of end-*gauche* defects in the solid monolayer, as would be expected from a comparison with bulk rotator phases.[42] SF spectra are insensitive to the presence of kinks, the other type of defect common in solid alkanes near the melting point. One feature of the SF spectra that is difficult to explain is the temperature dependence of I_{SF} (Fig. 5) which is approximately twice what we predict from the linear expansion coefficient measured by X-ray diffraction. Since the term A^{-2} in eqn. (10) is known from X-ray diffraction, the

discrepancy must lie in $\langle\beta\rangle$. Either the number of *gauche* defects must decrease rapidly as the temeprature is lowered or the tilt of the chains must change. The intensity of the d^+ mode in undecanol remained the same for 10 °C below T_m(2D), showing no indication of premelting.[16] If the chains are truly free to rotate about their axis, a small (5°) tilt would have a negligible (< 1%) effect on the SF intensity of the r^+ mode. As the lattice constant decreases, rotation becomes increasingly restricted and the chains are forced to adopt a well defined orientation with respect to their nearest neighbours. In a herring-bone arrangement a 5° tilt along the ***b***-axis would change the intensity by *ca.* 10%. Tilts of this order would be very difficult to detect by ellipsometry or X-ray diffraction. Some support for this possibility is presented by grazing incidence X-ray diffraction of uncompressed monolayers of tridecanol and tetradecanol spread on water at 5 °C.[5] These measurements reveal a distorted hexagonal unit cell with a chain tilt of 12° and 15°, respectively, but are consistent with a rotator phase as well as a herring-bone structure.

5.2 Liquid phase

IR spectra of liquid alkanes are dominated by localised modes, indicating the absence of long, all-*trans* segments.[41] The resulting loss of the local inversion symmetry gives rise to SF-active methylene modes. This effect is demonstrated in the SF spectrum of a monolayer of the non-ionic surfactant $CH_3(CH_2)_{11}(OC_2H_4)_3OH$, in which the methyl and methylene modes have comparable intensities (see inset in Fig. 3).[38] In the monolayers of alcohols on water, however, the d^+ mode is barely more intense in the 'liquid' phase than in the solid phase.[16,48] Thus the monolayers above T_m(2D) do not conform to our intuitive picture of a conformationally disordered liquid.

The monolayers of alcohols are essentially isostructural just below their phase-transition temperatures.[11–15] The volume per CH_2 in liquid alkanes just above their melting points is independent of chain length, suggesting similarities in local structure.[49] What would we expect to observe if the monolayers were isostructural above the phase transition also? Conformational defects aside, SF spectra depend on the number density and the orientation of the molecules, but not on the chain length. Therefore, we would expect the spectra above the phase transition to be the same, and ΔI_{SF} to be independent of chain length. The coefficient of ellipticity does depend on the thickness of the monolayer and we would expect $\Delta\bar{\rho}$ to be directly proportional to the chain length, after correcting for the effect of temperature on the relative permittivity of water. The observed values of ΔI_{SF} increase sharply from nonanol to undecanol and more slowly thereafter (Table 2). The jump in the ellipticity, $\Delta\bar{\rho}$, at the phase transition increases rapidly and monotonically with chain length. There is no evidence of either ΔI_{SF} or $\Delta\bar{\rho}$ tending towards limiting behaviour for long chains. Thus it is clear from even a qualitative analysis of the data that the structure of the liquid monolayer phase is strongly dependent on chain length.

The high degree of conformational order in the liquid phase suggested that we might successfully model the molecules as rigid rods. A combination of SFS and ellipsometry then allowed us to determine both the mean tilt, χ, of the chains (or more precisely, $\langle\cos\chi\rangle$) and the area per molecule, A. The plot of χ_l against A_l confirms the qualitative impression discussed above (Fig. 9). While the largest changes are seen between nonanol and undecanol, both χ_l and A_l continue to increase as the chain is made longer. From the values of χ_l and A_l, we can compute the density of the monolayer. In Fig. 11, we plot the volume per CH_2 against chain length. As Berge has noted before, the solid monolayer phase is less dense than the α (rotator) phase of crystalline alkanes or alcohols.[12] Conversely, the volume per CH_2 in the liquid monolayer is significantly less than in an alkane just above its melting point. The higher density in the liquid monolayer is reflected in the small amount of conformational disorder observed by SFS. The volume per CH_2 in the liquid monolayer increases with increasing chain length. This trend is consis-

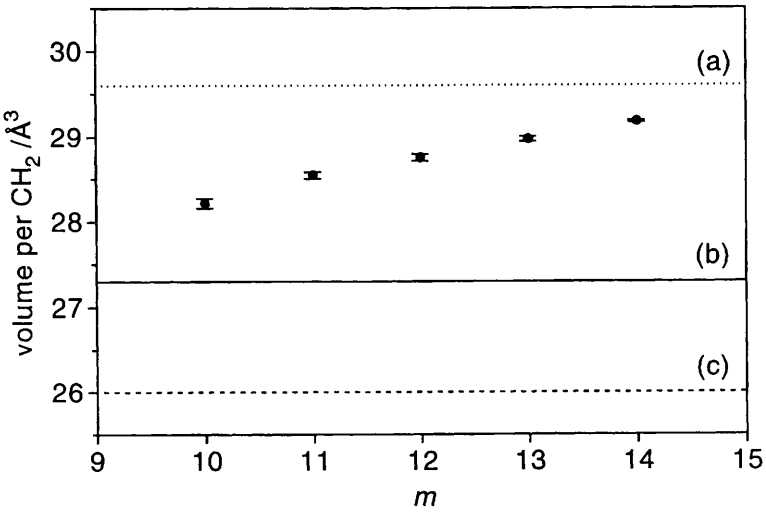

Fig. 11 Volume per CH_2 group in the liquid phase of monolayers of alcohols on water just above the phase transition temperature. Error bars at the 2σ level. The three lines represent the volume per CH_2 in (a) the liquid phase of bulk alkanes just above the melting point (····), (b) the solid phase of the monolayers, assuming $\chi_1 = 0°$ and $A_1 = 21.5$ Å^2 (——) and (c) the R_{II} phase of bulk alcohols (— —).[49]

tent with our observation that the methylene modes are more intense in the liquid phase of tetradecanol than undecanol.

In our analysis, we have neglected any increase in conformational disorder at T_m(2D). End-*gauche* defects reduce I_{SF}: an increase in these defects would shift the SF curves in Fig. 6 to the left. Kink defects reduce the length of the molecule by 1.3 Å but do not change the orientation of the terminal methyl groups. They, therefore, have little effect on the SF spectra but mimic the effect of a chain tilt on the ellipticity. An increase in kinks would shift the ellipticity curves in Fig. 6 to the right. Both types of defects would serve to reduce the chain tilt from the values in Table 3, but they have would have the opposite effect on A_1.

Chain defects and tilt disorder both contribute to the intrinsic roughness of the monolayer in the liquid phase. While σ_0 is likely to remain below the value in a liquid alkane ($\sigma_0 = 1.1$ Å),[50] part of the measured step $\Delta\bar{\rho}$ could nevertheless arise from $\bar{\rho}^R$ and not $\bar{\rho}^d$. A small increase in intrinsic roughness (*ca.* 0.5 Å r.m.s.) at T_m(2D) would be consistent with the X-ray reflection experiments of Rieu *et al.*[15] The effect of including a contribution from $\Delta\bar{\rho}^R$ is to increase the calculated density of the liquid phase: for dodecanol, a plausible value of $\Delta\bar{\rho}^R = +0.1 \times 10^{-3}$ would decrease the volume per CH_2 by 0.7% (*ca.* 0.2 Å^3).

On the basis of a thermodynamic analysis of surface tension,[14] Berge deduced that A_1 increased linearly with chain length, from 23.5 Å^2 for decanol to 27.5 Å^2 for tetradecanol. These values are much higher than those we measure and are difficult to reconcile with the SF data. Using our ellipticity data and a value of $A_1 = 27.5$ Å^2 for tetradecanol, we would expect $\Delta I_{SF} = 60\%$: much larger than the measured value of 37%. Given the way in which the ellipticity depends on χ_1 and A_1, it is, of course, possible to interpret our ellipticities within Berge's model. The results are still physically reasonable: the tilt increases from 19° for decanol to 32° for tetradecanol and the volume per CH_2 increases from 28.2 to 29.9 Å^3. The densities we determine are significantly lower than those deduced from X-ray reflectivity measurements, which is largely a

consequence of the model parameters chosen. The change in density at the phase transition is in good agreement with those measurements.[15]

5.3 Nonanol

The phase transition in nonanol appears to be associated with a small change in A and is therefore still weakly first-order. X-Ray measurements[13] show that the Bragg peak broadens throughout the region where we detect non-linear changes in the ellipticity, indicating a gradual decrease in the correlation length, and is still detectable at 0 °C. From our preliminary measurements, the tilts just above and just below the phase transition are indistinguishable. We cannot therefore rule out a continuous phase transition.

5.4 Comparison with bulk phases

The structure of the alcohol monolayers below T_m(2D) can be identified with the Rotator II phase, in the nomenclature of bulk alkanes, or the LS phase in the nomenclature of insoluble monolayers, although the area per chain is nearly 10% greater than is found in either of those systems.[49] The equivalent liquid crystal class would be smectic B. The solid phase of the alcohol does, however, have an unusually high temperature coefficient of expansion and the lattice parameters of the R_{II} and LS phases are approached at low temperatures.[12] Comparison with generic phase diagrams for insoluble monolayers would suggest the presence of an additional, second-order phase transition to a tilted phase as the chemical potential of the alcohol in solution is lowered.[6] X-Ray diffraction experiments on uncompressed monolayers of tridecanol and tetradecanol support an unusual structure in which the hexagonal unit cell is distorted towards the next-nearest neighbours and chains are tilted along the long, ***b***-axis of the unit cell.[5] While the surface pressure was not reported, one may assume that it was much lower than in monolayers in equilibrium with the bulk solid. IR spectra of a monolayer of $C_{16}OH$ on water also suggest a change from an upright to a tilted phase.[51] The phase transition between the upright and tilted phases has not itself been detected.

The label 'liquid' for the high-temperature phase is essentially a statement about the decay length of the translational correlation function. It says nothing about the local coordination of the molecules, the conformations of the chains, the magnitude or direction of the tilt of the chains or the persistence length of correlations in the tilt direction. Since the absence of Bragg peaks prevents analysis by X-ray diffraction, one has to study the liquid phase with other techniques. SF spectroscopy and ellipsometry have allowed us to calculate the density of the liquid phase and the magnitude of the mean chain tilt. The SF spectra also suggest that the chains remain largely *trans*-extended in the liquid just above the phase transition, though the occurrence of kink defects cannot be ascertained from the spectra. The persistence length associated with the direction of the chain tilt remains unknown. In a true liquid, the correlation in the tilt direction would show a rapid exponential decay. It also possible that the tilt correlation is long-range (algebraic decay in the correlation function). In this case, the high temperature phase is not a true liquid but a mesophase akin to the smectic C phase of liquid crystals. While an anisotropic fluid phase might seem unlikely, it has been postulated in phospholipid monolayers,[52] separated from the isotropic fluid by a further, second-order phase transition. Brewster angle microscopy would help to distinguish between these two phases.[53]

An obvious contrast between monolayers of alcohols and bulk, hydrated alcohols is the stability of rotator phases.[6,49] For the chain lengths studied here, the α-phase is thermodynamically stable for, at most, 12 K below the bulk melting point and for decanol the α-phase is not stable at any temperature.[54] Interactions between chains

favour an orthorhombic ⊥ subcell in which neighbouring chains are twisted at 90° to each other (herring-bone structure).[55] The O ⊥ subcell is the stable form of all the pure alcohols studied here. In the monolayers there is no evidence of a second phase transition at lower temperatures to a denser, herring-bone structure. Orthorhombic packing is, however, found in compressed monolayers of longer alcohols.[4] Thus, if the chain is sufficiently long, bulk effects overcome the interfacial effects that stabilise the rotator phase in shorter alcohols.

We speculate that the unusual stability of rotator phases in monolayers is a consequence of interfacial roughness. A feature of the high-temperature solid phases of alkanes (such as the R_{III} phase of tritriacontane)[35] is the presence of longitudinal disorder, *i.e.* correlated displacements in adjacent layers in a direction perpendicular to the layer plane. This type of disorder is absent in low temperature phases. In monolayers, capillary waves have the same effect as longitudinal disorder and, in the absence of rigidity, impose a roughness of the order of 5 Å r.m.s. on the monolayer. This roughness is not confined to long wavelengths, for example, the r.m.s. roughness with wavevectors between π/a and $\pi/2a$ is 1.2 Å.[32] In the monolayer rotator phase, the chains may be pictured as cylinders that can readily be displaced vertically with respect to their neighbours. In the herring-bone structure, adjacent chains interlock and vertical displacements result in van der Waals repulsions between adjacent chains. Stated differently, we would expect a densely packed herring-bone structure to have a high bending modulus that would suppress the capillary waves at high q.[56] Reducing interfacial roughness carries a large entropic penalty. For example, the entropy change associated with the formation of an interface between water and a hydrophobic surface (*e.g.* a hydrophobic solute) is large and negative,[57] yet the entropy of formation of a water/air interface is positive ($d\gamma/dT < 0$). The greater entropy associated with roughness at the air/water interface compared to the interlamellar interface in solid hydrocarbons would extend the range of stability of the rotator phase in monolayers.

6 Conclusion

The solid–liquid phase transition in monolayers of alcohols on water has been intensively studied over the past three years, but a number of questions about the structure of the liquid phase remain unanswered. We have used SFS to show that the density of isolated *gauche* defects does not increase greatly at the phase transition. Employing a model of the chains as rigid rods, we were then able to calculate the area per molecule and chain tilt in the liquid phase from a combination of sum-frequency and ellipsometric measurements. We found that the area per molecule and tilt increase monotonically with chain length. The decrease in density at the phase transition increased from 3% for decanol to 7% for tetradecanol, but the liquid monolayer remained denser than a bulk liquid alkane for all chain lengths.

A fully consistent interpretation of the ellipsometric data has been possible, incorporating both roughness and anisotropy. In the sum-frequency data, the temperature dependence of the SF signal in the solid phase is larger than expected, which is difficult to rationalise if the chains remain vertical and free to rotate as the temperature is lowered.

Close parallels between the behaviour of monolayers and bulk crystals exist. The unusual stability of rotator phases in monolayers compared to bulk phases may have its origin in interfacial roughness.

Note added in proof

We have recently discovered that a phase transition in a monolayer of tetradecanol on water was observed by Trapeznikov as long ago as 1945 in surface viscosity and surface tension measurements.[67] Surface viscosity measurements on the monolayers of the alco-

hols $CH_3(CH_2)_{m-1}OH$ (m = 10, 12, 14 and 16) by Ross in 1957 also indicated a phase transition.[68] The two-dimensional phase transition temperatures reported by Trapeznikov and Ross agree well with recent results.

We thank the EPSRC for financial support, Unilever Research (Port Sunlight Laboratory) for a CASE award to B.D.C., and the European Union for an HCM Fellowship to R.B.

Appendix: Sample heating by IR laser beam

1 Steady-state heating

In the absence of convection, the steady-state temperature rise, ΔT, due a point source of strength, S(mW), at the surface of water is given by

$$\Delta T = 0.27 \frac{S}{r} \tag{A1}$$

where r is the radial distance from the source in mm. We can approximate the experimental situation to a hemispherical source with a circular cross-section equal in area to that of the IR laser beam. For r = 0.2 mm and S = 20 mW, ΔT = 27 K. Such a large temperature rise, coupled with the r^{-1} dependence of ΔT, produces steep density and surface-tension gradients, which rapidly cause a convection cell to develop.[58] Convection was readily observed in a cloudy suspension of alcohol droplets in water. Since $d\gamma/dT$ is, unusually, positive for alcohol monolayers on water, Bénard (surface-tension driven) and Rayleigh (buoyancy driven) convection cells will flow in opposite directions. It would be interesting to observe which effect dominates.

To minimise the effect of steady-state heating, we rotate the sample cell continuously and illuminate a spot on the surface at a distance R from the axis of rotation. The rotation rate (14 rpm) is chosen so that successive pulses from the IR laser do not overlap. For $r \ll R$, the system can be treated as a line source of strength $S/2\pi R$ mW mm^{-1}. We then find that

$$\Delta T = 0.086 \frac{S}{R} \ln(l_{max}/r) \tag{A2}$$

where the upper cut-off, $l_{max} \approx 1$ cm, is determined by distance to the sides of the cell, which are held at a constant temperature. For S = 20 mW, R = 15 mm and r = 0.2 mm as before, ΔT = 0.4 K. As the temperature profile varies only logarithmically with distance, the density and surface-tension gradients that lead to convection are further reduced.

The temperature of the liquid is measured at the same distance, R, as the laser spot from the axis of rotation, with a thermocouple protruding *ca.* 0.5 mm beneath the surface of the water. With this arrangement the measured temperature should agree with the average temperature within the IR laser spot to an accuracy of 0.1 K.

2 Transient heating

The length of the IR pulse is *ca.* 1 ns. The thermal diffusion length, $l_D = (4kt)^{1/2}$, in water and hydrocarbons in 1 ns is 24 and 17 nm, respectively (where k is the thermal diffusivity). Since the vibrational relaxation time (*ca.* ps)[59] is much shorter than the pulse length, and the thickness of the monolayer (1–2 mm) is much less than l_D, the monolayer is thermally equilibrated with the water immediately beneath the surface.

The temperature rise in the monolayer caused by the IR laser pulse arises from direct absorption by the monolayer and from absorption by the water beneath.

(a) Monolayer absorption. Since the radius, r, of the IR spot is very much greater than l_D, the monolayer acts as a planar heat source of strength ΔI, where $f = \Delta I/I$ is the fraction of the laser beam absorbed by the monolayer and I is the intensity of the laser

pulse. To estimate the temperature rise we treat the laser pulse as instantaneous and calculate the temperature rise after 1 ns. A more accurate estimate of ΔT could be derived from the equations of Bechtel[60] for Gaussian pulses, but such accuracy is not necessary here. The surface temperature rise at time, t, due to an instantaneous planar heat source of strength ΔI is[61]

$$\Delta T = \frac{\Delta I}{U\sqrt{(\pi t)}} \tag{A3}$$

where U is the thermal effusivity and has a value of 1.6×10^3 J m^{-2} K^{-1} s$^{-1/2}$ for water at 298 K. We estimate $f \approx 10^{-4}$ at the peak of the CH_2 absorption, yielding $\Delta T \approx 6$ K after 1 ns for an intensity $I = 5$ kJ m^{-2} (0.7 mJ pulse^{-1}, $r = 0.2$ mm). At a wavelength of 2880 cm^{-1} (CH_3 symmetric stretch) the IR absorption is much weaker and $\Delta T \approx 1$ K.

(b) Water absorption. Since the attenuation length, $1/\alpha$, of the IR radiation in water is very much greater than l_D, we can ignore diffusion on the timescale of the laser pulse. The temperature rise at the surface of water is

$$\Delta T = 2.4 \times 10^{-7} \alpha I \tag{A4}$$

where α is in m^{-1} and I is in J m^{-2}. At a wavenumber of 2880 cm^{-1} and with other parameters as before, we find $\Delta T = 12$ K for a subphase of D_2O and 50 K for H_2O.[62] The temperature of the monolayer is therefore determined principally by water absorption. Near 3000 cm^{-1}, where α for H_2O is higher, local boiling of the surface of H_2O is observed. D_2O was used throughout these experiments.

3 Effect on spectra

The phase transition is accompanied by a change in surface coverage. Evaporation and dissolution rates are entirely negligible on the nanosecond timescale. The speed of compressional waves places an upper limit on the rate at which a density fluctuation could be transmitted across the monolayer. The speed of sound in water is 1.5×10^3 m s^{-1}: it would take hundreds of nanoseconds to transport material out of the irradiated area. Transient heating does not change the area per molecule.

While 1 ns is a very short time for transport of molecules away from the interface, it is long enough to equilibrate at least some of the molecular degrees of freedom in the film. Molecular dynamics simulations of dense chain systems at room temperature and at a constant density typically reach equilibrium in 100 ps.[63] On the timescale of 1 ns, collective reorientation of the tilt angle and direction are observed in addition to intramolecular motions, such as chain rotation and conformational isomerisation.[64] Experimentally, however, we have observed that SF spectra taken 1 and 8 K below the phase-transition temperature are indistinguishable, with the exception of a small overall intensity factor. This observation suggests that, at least below T_m(2D), the monolayer structure is determined principally by the area per molecule and is insensitive to small changes in the temperature at constant density. Relatively few monolayer simulations have focused on the effect of temperature at constant density. In one such simulation[65] of a sixteen-carbon chain at an area per molecule of 21.4 Å^2 (very similar to the condensed phase of the *n*-alcohols on water), only small changes in tilt ($< 1°$) and *gauche* defect density ($< 1\%$) were associated with a 10 K rise in temperature.

References

1 A. Pockels, *Nature (London)*, 1891, **43**, 437.
2 I. Langmuir, *J. Am. Chem. Soc.*, 1917, **39**, 1848.
3 See, *e.g.* (*a*) N. K. Adam, *Proc. R. Soc.*, 1922, **101**, 516; (*b*) W. D. Harkins and L. E. Copeland, *J. Chem. Phys.*, 1942, **10**, 242; (*c*) D. G. Dervichian, *J. Chem. Phys.*, 1939, **7**, 931; (*d*) S. Ställberg-Stenhagen and E. Stenhagen, *Nature (London)*, 1945, **156**, 239; (*e*) G. L. Gaines, *Insoluble Monolayers at Liquid-Gas Interfaces*, Wiley, New York, 1966; (*f*) M. Lundquist, *Chem. Scr.*, 1971, **1**, 5; (*g*) S. R. Middleton and B. A.

Pethica, *Faraday Symp. Chem. Soc.*, 1981, **16**, 109; (*h*) A. M. Bibo, C. M. Knobler and I. R. Peterson, *J. Phys. Chem.*, 1991, **95**, 5591.
4 K. Kjaer, J. Als-Nielsen, C. A. Helm, L. A. Laxhuber and H. Möhwald, *Phys. Rev. Lett.*, 1987, **58**, 2224; P. Dutta, J. B. Peng, B. Lin, J. B. Ketterson, M. Prakash, P. Georgopoulos and S. Ehrlich, *Phys. Rev. Lett.*, 1987, **58**, 2228; J. Als-Nielsen, D. Jacquemain, K. Kjaer, F. Leveiller, M. Lahav and L. Leiserowitz, *Phys. Rep.* 1994, **246**, 251. For studies on long-chain alcohols, see J. L. Wang, F. Leveiller, D. Jacquemain, K. Kjaer, J. Als-Nielsen, M. Lahav and L. Leiserowitz, *J. Am. Chem. Soc.*, 1994, **116**, 1192; D. Jacquemain, F. Leveiller, S. P. Weinbach, M. Lahav, L. Leiserowitz, K. Kjaer and J. Als-Nielsen, *J. Am. Chem. Soc.*, 1991, **113**, 7684; R. Popovitz-Biro, J. L. Wang, J. Majewski, E. Shavit, L. Leiserowitz and M. Lahav, *J. Am. Chem. Soc.*, 1994, **116**, 1179; S. W. Barton, B. N. Thomas, E. B. Flom, S. A. Rice, B. Lin, J. B. Peng, J. B. Ketterson and P. Dutta, *J. Chem. Phys.*, 1988, **89**, 2257; M. C. Shih, T. M. Bohanon, J. M. Mikrut, P. Zschack and P. Dutta, *J. Chem. Phys.*, 1992, **97**, 4485.
5 J. Majewski, R. Popovitz-Biro, W. G. Bouwman, K. Kjaer, J. Als-Nielsen, M. Lahav and L. Leiserowitz, *Chem. Eur. J.*, 1995, **1**, 304.
6 I. R. Peterson, V. Brzezinski, R. M. Kenn and R. Steitz, *Langmuir*, 1992, **8**, 2995; I. R. Peterson and R. M. Kenn, *Langmuir*, 1994, **10**, 4645.
7 J. C. Earnshaw, C. P. Nugent, K. Lunkenheimer and R. Hirte, *J. Phys. Chem.*, 1996, **100**, 5004.
8 G. A. Lawrie and G. T. Barnes, *J. Colloid Interface Sci.*, 1994, **162**, 36; S. R. Middleton, M. Iwahashi, N. R. Pallas and B. A. Pethica, *Proc. R. Soc. London, Ser. A*, 1984, **396**, 143.
9 N. R. Pallas and B. A. Pethica, *J. Chem. Soc., Faraday Trans. 1*, 1987, **83**, 585.
10 M. Aratono, S. Uryu, Y. Hayami, K. Motomura and R. Matuura, *J. Colloid Interface Sci.*, 1984, **98**, 33.
11 B. Berge and A. Renault, *Europhys. Lett.*, 1993, **21**, 773.
12 A. Renault, J. F. Legrand, M. Goldmann and B. Berge, *J. Phys. II France*, 1993, **3**, 761.
13 J. F. Legrand, A. Renault, O. Konovalov, E. Chevigny, J. Als-Nielsen, G. Grübel and B. Berge, *Thin Solid Films*, 1994, **248**, 95.
14 B. Berge, O. Konovalov, J. Lajzerowicz, A. Renault, J. P. Rieu and M. Vallade, *Phys. Rev. Lett.*, 1994, **73**, 1652.
15 J. P. Rieu, J. F. Legrand, A. Renault, B. Berge, B. M. Ocko, X. Z. Wu and M. Deutsch, *J. Phys. II France*, 1995, **5**, 607.
16 R. Braun, B. D. Casson and C. D. Bain, *Chem. Phys. Lett.*, 1995, **245**, 326.
17 M. Lin, J-L. Firpo, P. Mansoura and J. F. Baret, *J. Chem. Phys.*, 1979, **71**, 2202; M. Aratono, T. Takiue, N. Ikeda, A. Nakamura and K. Motomura, *J. Phys. Chem.*, 1992, **96**, 9422; 1993, **97**, 5141; J. Glinski, G. Chavepeyer, J. K. Platten and C. de Saedeleer, *J. Colloid Interface Sci.*, 1993, **158**, 382; M. Salajan, J. Glinski, G. Chavepeyer and J. K. Platten, *J. Colloid Interface Sci.*, 1994, **164**, 387.
18 R. N. Ward, PhD Thesis, Cambridge University, 1993; M. S. Johal, E. W. Usadi and P. B. Davies, *J. Chem. Soc., Faraday Trans.*, 1996, **92**, 573.
19 X. Z. Wu, E. B. Sirota, S. K. Sinha, B. M. Ocko and M. Deutsch, *Phys. Rev. Lett.*, 1994, **70**, 958.
20 B. Berge, L. Faucheux, K. Schwab and A. Libchaber, *Nature (London)*, 1991, **350**, 322.
21 D. Zhang, J. H. Gutow, K. B. Eisenthal and T. F. Heinz, *J. Chem. Phys.*, 1993, **98**, 5099; D. Zhang, J. H. Gutow and K. B. Eisenthal, *J. Chem. Soc., Faraday Trans.*, 1996, **92**, 539.
22 J. H. Hunt, P. Guyot-Sionnest and Y. R. Shen, *Chem. Phys. Lett.*, 1987, **133**, 189.
23 Y. R. Shen, *Principles of Nonlinear Optics*, Wiley, New York, 1984; Y. R. Shen, *Nature (London)*, 1989, **337**, 519; K. B. Eisenthal, *Annu. Rev. Phys. Chem.*, 1992, **43**, 627; K. B. Eisenthal, *Acc. Chem. Res.*, 1993, **26**, 636.
24 C. D. Bain, *J. Chem. Soc., Faraday Trans.*, 1995, **91**, 1281.
25 For example, Ch. Bouhet, *Ann. Phys. (Paris)*, 1931, **15**, 5; E. Hofmeister, *Z. Phys.*, 1953; **136**, 137; D. den Engelsen and B. de Koning, *J. Chem. Soc., Faraday Trans.*, 1974, **70**, 1603; Th. Rasing, H. Hsiung, Y. R. Shen and M. W. Kim, *Phys. Rev. A*, 1988, **37**, 2732; M. W. Kim, B. B. Sauer, H. Yu, M. Yazdanian and G. Zografi, *Langmuir*, 1990, **6**; 236. D. Ducharme, J-J. Max, C. Salesse and R. M. Leblanc, *J. Phys. Chem.*, 1990, **94**, 1925.
26 M. Paudler, J. Ruths and H. Riegler, *Langmuir* 1992, **8**, 184.
27 J. Meunier, *J. Phys (Paris)*, 1987, **48**, 1819.
28 M. J. Dignam, M. Moskovitts and R. W. S obie, *Trans. Faraday Soc.*, 1971, **67**, 3306; D. den Engelson, *J. Opt. Soc. Amer.*, 1971, **61**, 1460.
29 D. Beaglehole, in *Fluid Interfacial Phen mena*, ed. C. A. Croxton, Wiley, 1986, p. 523; J. Lekner, *Theory of Reflection*, Nijhoff, Dordrecht, 1987.
30 P. Drude, *Ann. Phys. Chem. (Leipzig)*, 1991, **43**, 126.
31 J. Meunier, in *Light Scattering by Liquid Surfaces and Complementary Techniques*, ed. D. Langevin, Marcel Dekker, New York, 1992, ch. 17.
32 P. Croce, *J. Optics (Paris)*, 1977, **8**, 127; 1990, **21**, 273.
33 D. Beaglehole, *Physica B*, 1980, **100**, 163.
34 B. J. A. Zielinska, D. Bedeaux and J. Vliegler, *Physica A*, 1981, **107**, 91.
35 B. Ewen, G. R. Strobl and D. Richter, *Faraday Discuss.*, 1980, **69**, 19; J. P. Ryckaert, M. L. Klein and I. R. MacDonald, *Phys. Rev. Lett.*, 1987, **58**, 698.

36 C. J. F. Böttcher, *Theory of Electric Polarization*, Elsevier, Amsterdam, 2nd edn., 1973; J. Zyss and D. S. Chemla, *Nonlinear Optical Properties of Organic Molecules and Crystals*, Academic, Orlando, 1987.
37 H. Bercegol, F. Gallet, D. Langevin and J. Meunier, *J. Phys. (Paris)*, 1989, **50**, 2277.
38 G. R. Bell, C. D. Bain and R. N. Ward, *J. Chem. Soc., Faraday Trans.*, 1996, **92**, 515.
39 C. D. Bain, P. B. Davies, T. H. Ong, R. N. Ward and M. A. Brown, *Langmuir*, 1991, **7**, 1563.
40 R. G. Snyder, H. L. Strauss and C. A. Elliger, *J. Phys. Chem.*, 1982, **86**, 5145; R. A. MacPhail, H. L. Strauss, R. G. Snyder and C. A. Elliger, *J. Phys. Chem.*, 1984, **88**, 334; R. N. Ward, D. C. Duffy, P. B. Davies and C. D. Bain, *J. Phys. Chem.*, 1994, **98**, 8536.
41 M. Maroncelli, S. P. Qi, H. L. Strauss and R. G. Snyder, *J. Am. Chem. Soc.*, 1982, **104**, 6237; R. G. Snyder, M. Maroncelli, H. L. Strauss, C. A. Elliger, D. G. Cameron, H. L. Casal and H. H. Mantsch, *J. Am. Chem. Soc.*, 1983, **105**, 133; M. Maroncelli, H. L. Strauss and R. G. Snyder, *J. Chem. Phys.*, 1985, **82**, 2811; Y. Kim, H. L. Strauss and R. G. Snyder, *J. Phys. Chem.*, 1989, **93**, 7520.
42 C. Hirose, N. Akamatsu and K. Domen, *Appl. Spectrosc*, 1992, **42**, 1051.
43 K. Wolfrum and A. Laubereau, *Chem. Phys. Lett.*, 1994, **228**, 83; C. Hirose, N. Akamatsu and K. Domen, *J. Chem. Phys.*, 1992, **96**, 997; C. Hirose, H. Yamamoto, N. Akamatsu and K. Domen, *J. Phys. Chem.*, 1993, **39**, 10064.
44 *Handbook of Chemistry and Physics*, ed. R. C. Weast, CRC Press, Boca Raton, 64th edn., 1983.
45 A. I. Vogel, *J. Chem. Soc.*, 1946, 133.
46 *Polymer Handbook*, ed. J. Brandrup and E. H. Immergut, Wiley, New York, 3rd edn., 1989, p. V/20.
47 L. T. Lee, D. Langevin, J. Meunier, K. Wong and B. Cabane, *Prog. Colloid Polym. Sci.*, 1990, **81**, 209; J. Meunier and L. T. Lee, *Langmuir*, 1991, **7**, 1855.
48 G. A. Sefler, Q. Du, P. B. Miranda and Y. R. Shen, *Chem. Phys. Lett.*, 1995, **235**, 347.
49 D. M. Small, *The Physical Chemistry of Lipids*, Plenum, New York, 1986, ch. 8.
50 B. M. Ocko, X. Z. Wu, E. B. Sirota, S. K. Sinha and M. Deutsch, *Phys. Rev. Lett.*, 1994, **72**, 242.
51 A. Gericke, J. Simon-Kutscher and H. Hühnerfuss, *Langmuir*, 1993, **9**, 3115.
52 O. Albrecht, H. Gruler and E. Sackmann, *J. Physique*, 1978, **39**, 301.
53 G. A. Overbeck, D. Hönig and D. Möbius, *Langmuir*, 1993, **9**, 555.
54 A. S. C. Lawrence, M. A. Al-Mamun and M. P. McDonald, *Trans. Faraday Soc.*, 1967, **63**, 2789; C. Mosselman, J. Mourik and H. Dekker, *J. Chem. Thermodynam.*, 1974, **6**, 477.
55 S. Abrahamsson, B. Dahlén, H. Löfgren and I. Pascher, *Prog. Chem. Fats Lipids*, 1978, **16**, 125.
56 J. Daillant, L. Bosio, J. J. Benattar and J. Meunier, *Europhys. Lett.*, 1989, **8**, 453.
57 C. Tanford, *The Hydrophobic Effect*, Wiley, New York, 2nd edn., 1980.
58 R. F. Probstein, *Physicochemical Hydrodynamcs*, Wiley, New York, 2nd edn., 1994, p. 352.
59 A. L. Harris and N. J. Levinos, *J. Chem. Phys.*, 1989, **90**, 3878; A. L. Harris, L. Rothberg, L. Dhar, N. J. Levinos and L. H. Dubois, *J. Chem. Phys.*, 1991, **94**, 2438.
60 J. H. Bechtel, *J. Appl. Phys.*, 1975, **46**, 1585.
61 C. D. Bain, P. B. Davies and T. H. Ong, *Chem. Phys. Lett.*, 1992, **194**, 391.
62 J. E. Bertie, M. K. Ahmed and H. E. Eysel, *J. Phys. Chem.*, 1989, **93**, 2210.
63 See, for example, J. Harris and S. A. Rice, *J. Chem. Phys.*, 1988, **89**, 5898; S. Karaborni, S. Toxvaerd and O. H. Olsen, *J. Phys. Chem.*, 1992, **96**, 4965; M. L. Klein, *J. Chem. Soc., Faraday Trans.*, 1992, **88**, 1701.
64 M. A. Moller, D. J. Tildesley, K. S. Kim and N. Quirke, *J. Chem. Phys.*, 1991, **94**, 8390.
65 J. Hautmann and M. L. Klein, *J. Chem. Phys.*, 1990, **93**, 7483.
66 J. R. Lu, M. Hromadova, R. K. Thomas and J. Penfold, *Langmuir*, 1993, **40**, 247.
67 A. Trapeznikov, *Acta Physicochim. URSS*, 1945, **20**, 589.
68 J. Ross, *J. Phys. Chem.*, 1958, **62**, 531.

Paper 6/03667H; *Received* 28*th May*, 1996